



Article

# Pybox-Iron(II) Spin-Crossover Complexes with Substituent Effects from the 4-Position of the Pyridine Ring (Pybox = 2,6-Bis(oxazolin-2-yl)pyridine)

Akifumi Kimura and Takayuki Ishida \*

Department of Engineering Science, The University of Electro-Communications, Chofu, Tokyo 182-8585, Japan; kimura@tff.pc.uec.ac.jp

\* Correspondence: takayuki.ishida@uec.ac.jp; Tel.: +81-42-443-5490; Fax: +81-42-443-5501

Received: 30 June 2017; Accepted: 31 July 2017; Published: 8 August 2017

**Abstract:** Spin-crossover (SCO) behavior of a series of  $[\text{Fe}(\text{X-pybox})_2](\text{ClO}_4)_2$  was investigated, where X-pybox stands for 4-X-substituted 2,6-bis(oxazolin-2-yl)pyridine with X = H, Cl, Ph,  $\text{CH}_3\text{O}$ , and  $\text{CH}_3\text{S}$ . We confirmed that the mother compound  $[\text{Fe}(\text{H-pybox})_2](\text{ClO}_4)_2$  underwent SCO above room temperature. After X was introduced, the SCO temperatures ( $T_{1/2}$ ) were modulated as 310, 230, and 330 K for X = Cl, Ph, and  $\text{CH}_3\text{S}$ , respectively. The  $\text{CH}_3\text{O}$  derivative possessed the high-spin state down to 2 K. Crystallographic analysis for X = H, Cl,  $\text{CH}_3\text{O}$ , and  $\text{CH}_3\text{S}$  was successful, being consistent with the results of the magnetic study. Distorted coordination structures stabilize the HS (high-spin) state, and the highest degree of the coordination structure distortion is found in the  $\text{CH}_3\text{O}$  derivative. A plot of  $T_{1/2}$  against the Hammett substituent constant  $\sigma_p$  showed a positive relation. Solution susceptometry was also performed to remove intermolecular interaction and rigid crystal lattice effects, and the  $T_{1/2}$ 's were determined as 260, 270, 240, 170, and 210 K for X = H, Cl, Ph,  $\text{CH}_3\text{O}$ , and  $\text{CH}_3\text{S}$ , respectively, in acetone. The substituent effect on  $T_{1/2}$  became very distinct, and it is clarified that electron-donating groups stabilize the HS state.

**Keywords:** spin crossover; spin transition; iron(II) ion; crystal structure

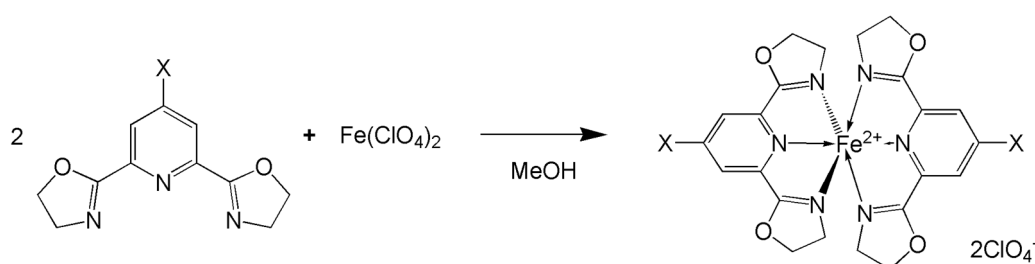
## 1. Introduction

Spin-crossover (SCO) is a reversible transition between low-spin (LS) and high-spin (HS) states by external stimuli like heat, light, pressure, or magnetic field [1–7]. Iron(II) ( $3d^6$ ) coordination compounds attract a great deal of attention in various SCO complexes, because SCO takes place between dia- and paramagnetic states to show drastic change in magnetic and chromic properties. The six-nitrogen donor structures (i.e.,  $\text{Fe}^{\text{II}}\text{N}_6$ ) have been studied extensively, and in particular diimines like 2-pyridylmethyleimine and bipyridyl derivatives [8–13] and triimines like 2,6-bis(azaaryl)pyridine derivatives and tripodal tris(azaaryl) compounds [14–19] are the most popular ligands for this purpose. The structural similarity found between the meridional SCO ligands 1-bpp [14] and 3-bpp [15] (2,6-bis(pyrazol-1-yl)- and 2,6-bis(pyrazol-3-yl)pyridine, respectively) affords us a clue for the development of robust SCO ligands with respect to the ligand-field engineering.

In this study, the synthesis and physical properties of  $\text{Fe}^{2+}$  complexes were investigated (Scheme 1), in which pybox (2,6-bis(oxazolin-2-yl)pyridine) ligands were involved as a triimine ligand. The pybox coordination compounds have been intensively studied for various reaction catalysts often carrying a chiral center in the oxazoline rings [20,21] and luminescent lanthanoid complexes as relatively recent topics [22–24]. More recently, Gao et al. explored the SCO application of pybox-iron(II) systems; the mother X = H compound  $[\text{Fe}(\text{pybx})_2](\text{ClO}_4)_2$  [25] and a tetramethylated compound  $[\text{Fe}(\text{L})_2](\text{ClO}_4)_2$  (L = 2,6-bis(4,4-dimethyloxazolin-2-yl)pyridine) [26] underwent SCO around  $T_{1/2} = 345$  and 162–176 K, respectively, with attention concentrated on the solvent and counter anion dependence. Furthermore,

Halcrow et al. reported that chiral (*S,S*)- or (*R,R*)-4,4'-dimethylated derivatives were subjected to the SCO study [27]. On the other hand, we are now focusing on intramolecular substituent effects, because the introduction of substituents would bring about drastic SCO tuning through the covalent bonds, rather than through van der Waals interaction. Furthermore, the physical properties should be designed and controlled in a non-serendipitous way.

We planned to modulate the SCO temperature with the aid of electronic and steric effects from a substituent group which is bound at the 4-position of the pyridine ring. The electronic substituent effects will be mainly discussed in this work, since the steric effects are hardly parameterized. After the difference of crystal packing motif is ignored, the Hammett substituent constants were applied to the relationship analysis. A role of the coordination structure distortion will be clarified. At the next stage, solution susceptometry was performed to remove intermolecular interaction and rigid crystal lattice effects. The intrinsic substituent dependence on the SCO behavior will be revealed, as discussed in connection with the known parallel results on the SCO complexes having a related meridional ligand.



**Scheme 1.** Synthesis of  $[\text{Fe}(\text{X-pybox})_2](\text{ClO}_4)_2$  ( $\text{X} = \text{H}, \text{Cl}, \text{Ph}, \text{CH}_3\text{O}, \text{CH}_3\text{S}$ ). Pybox: (2,6-bis(oxazolin-2-yl)pyridine).

## 2. Results

### 2.1. Preparation

New compounds  $[\text{Fe}(\text{X-pybox})_2](\text{ClO}_4)_2$  ( $\text{X} = \text{Cl}, \text{Ph}, \text{CH}_3\text{O}, \text{CH}_3\text{S}$ ) were prepared according to the conventional method [23,28–30]. All the ligands were known, except for  $\text{X} = \text{CH}_3\text{S}$ . The complex formation using  $\text{Fe}(\text{ClO}_4)_2 \cdot 6\text{H}_2\text{O}$  was conducted in methanol. The resulting dark red polycrystalline compound was isolated on a filter, and the product was purified by recrystallization from methanol. The elemental and spectroscopic analyses supported the formula of  $[\text{Fe}(\text{X-pybox})_2](\text{ClO}_4)_2$ . Solvated molecules were found in the  $\text{X} = \text{Ph}$  and  $\text{CH}_3\text{S}$  case.

### 2.2. Crystal Structures

The X-ray crystallographic analysis on  $[\text{Fe}(\text{X-pybox})_2](\text{ClO}_4)_2$  ( $\text{X} = \text{H}, \text{Cl}, \text{CH}_3\text{O}, \text{CH}_3\text{S}$ ) was successful at 100 and/or 400 K (Table 1 and Figure 1). The crystal structure of the mother compound  $[\text{Fe}(\text{H-pybox})_2](\text{ClO}_4)_2$  at 173 K has already been reported [25]; the crystal system is monoclinic  $P2_1/n$  with  $a = 15.386(3)$ ,  $b = 10.700(2)$ ,  $c = 16.934(3)$  Å,  $\beta = 103.31(3)^\circ$ , and  $V = 2713.2(10)$  Å<sup>3</sup>. We determined the crystal structure of this compound at 400 K as well as 100 K. The space group was kept at 400 K, and the cell volume was enlarged by 8.4% (Table 1). The Fe–N distances are listed in Table 2, and suggest that the population is almost shifted to the HS state at 400 K.

The space group of the  $[\text{Fe}(\text{Cl-pybox})_2](\text{ClO}_4)_2$  crystal is  $P2_1/c$ , and there is a unique crystallographically-independent molecule in a unit cell. The cell parameters (Table 1) were converted to a space group  $P2_1/n$  to give  $a = 19.314(3)$ ,  $b = 11.170(2)$ ,  $c = 14.787(2)$  Å, and  $\beta = 103.31(3)^\circ$  at 100 K. The molecular arrangement motif is different from that of  $[\text{Fe}(\text{H-pybox})_2](\text{ClO}_4)_2$ . The Fe–N bond lengths (Table 2) guarantee the LS state at 100 K. The crystal structure at 400 K was also determined. The space group was maintained, and the cell volume was somewhat enlarged by 7.5% (Table 1). The

Fe–N bond lengths were elongated by 10% (Table 2). This finding suggests that most of the population occupies the HS state at 400 K.

**Table 1.** Selected crystallographic parameters of  $[\text{Fe}(\text{X-pybox})_2](\text{ClO}_4)_2$  ( $\text{X} = \text{H}, \text{Cl}, \text{CH}_3\text{O}, \text{CH}_3\text{S}$ ).

X	H	Cl	Cl	CH <sub>3</sub> O	CH <sub>3</sub> S
T/K	400	100	400	100	100
Formula weight	689.20	758.09	758.09	749.25	845.46
Crystal system	monoclinic	monoclinic	monoclinic	monoclinic	orthorhombic
Space group	$P2_1/n$	$P2_1/c$	$P2_1/c$	$Cc$	$P2_12_12_1$
$a/\text{Å}$	16.140(3)	14.787(2)	15.857(4)	12.084(3)	12.656(3)
$b/\text{Å}$	10.9603(17)	11.170(2)	10.588(3)	12.822(3)	15.676(4)
$c/\text{Å}$	17.049(3)	18.164(3)	19.084(4)	19.328(5)	16.897(4)
$\beta/^\circ$	102.736(9)	109.071(8)	107.947(11)	101.716(12)	90.
$V/\text{Å}^3$	2941.8(9)	2835.4(8)	3048.1(13)	2932.3(12)	3352.1(13)
Z	4	4	4	4	4
$d_{\text{calcd.}}/\text{g}\cdot\text{cm}^{-3}$	1.556	1.776	1.652	1.697	1.675
$\mu$ (MoK $\alpha$ )/ $\text{mm}^{-1}$	0.763	0.983	0.914	0.778	0.811
No. of unique reflections	5760	6481	6966	6488	7660
$R$ ( $F$ ) ( $I > 2\sigma(I)$ ) <sup>a</sup>	0.0830	0.0698	0.0830	0.0361	0.0503
$wR$ ( $F^2$ ) (all reflections) <sup>b</sup>	0.2959	0.1978	0.2863	0.0908	0.1193
Goodness-of-fit parameter	0.981	1.047	1.009	1.052	1.068
Flack parameter	-	-	-	-0.008(4)	0.002(9)

$$^a R = \sum[|F_o| - |F_c|]/\sum|F_o|; ^b wR = [\sum w(F_o^2 - F_c^2)/\sum wF_o^4]^{1/2}.$$

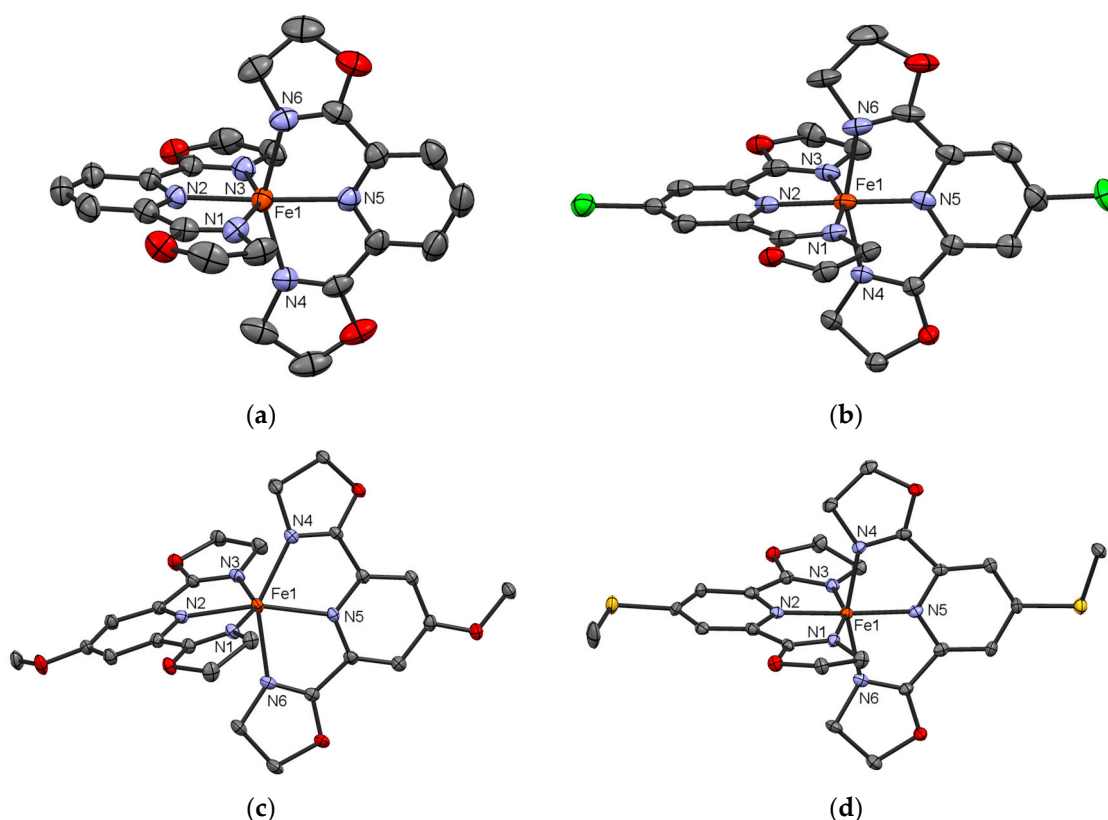


**Figure 1.** X-ray crystal structures of  $[\text{Fe}(\text{X-pybox})_2](\text{ClO}_4)_2$  for  $\text{X} =$  (a) H (400 K); (b) Cl (100 K); (c) CH<sub>3</sub>O (100 K); and (d) CH<sub>3</sub>S (100 K). The thermal ellipsoids are drawn at the 20%, 50%, 50%, and 50% probability levels, respectively. Hydrogen atoms and counter anions are omitted for clarity.

The space group of the crystal of  $[\text{Fe}(\text{CH}_3\text{O-pybox})_2](\text{ClO}_4)_2$  is monoclinic  $Cc$ , and the Flack parameter was satisfactorily reduced. There is a unique crystallographically-independent molecule in a unit cell. The molecular packing motif is completely different from those of the H and Cl derivatives.

From the Fe–N bond lengths (Table 2), the state is suggested to be HS. Table 3 summarizes the N–Fe–N bond angles. As a common feature, the N–Fe–N bite angles are largely deviated from the right angle owing to the five-membered chelate rings. However, the molecular structure of the CH<sub>3</sub>O derivative clearly exhibits a bent N(py)–Fe–N(py) axis (the angle of 156.74(12)°) (Figure 1c). In contrast, the 400 K structures of the X = H and Cl derivatives show practically linear N(py)–Fe–N(py) axes (177.6(2) and 176.50(15)°, respectively).

Compound [Fe(CH<sub>3</sub>S-pybox)<sub>2</sub>](ClO<sub>4</sub>)<sub>2</sub> crystallizes in a space group orthorhombic *P*2<sub>1</sub>2<sub>1</sub>2<sub>1</sub>. The Flack parameter was satisfactorily reduced. There is a unique crystallographically-independent molecule. The crystal involves two molar methanol molecules; namely, the composition formula is [Fe(CH<sub>3</sub>S-pybox)<sub>2</sub>](ClO<sub>4</sub>)<sub>2</sub>(CH<sub>3</sub>OH)<sub>2</sub>, being consistent with the results of the elemental analysis and magnetic measurements (see below). From the Fe–N bond lengths (Table 2), the state is suggested to be LS at 100 K. The molecular structure (Figure 1d) displays a relatively linear N(py)–Fe–N(py) axis (176.62(19)°), as usually found in the LS molecules of this family. At high temperatures (e.g., 400 K), the crystals were broken down and the crystal structure analysis was unsuccessful. The elemental analysis suggests that some methanol molecules would be liberated from the crystal lattice.

**Table 2.** Fe–N bond distances (*d*) in Å for [Fe(X-pybox)<sub>2</sub>](ClO<sub>4</sub>)<sub>2</sub> (X = H, Cl, CH<sub>3</sub>O, CH<sub>3</sub>S).

X	H (400 K)	Cl (100 K)	Cl (400 K)	CH <sub>3</sub> O (100 K)	CH <sub>3</sub> S (100 K)
<i>d</i> (Fe1–N1)	2.134(6)	1.956(4)	2.153(4)	2.209(3)	1.991(4)
<i>d</i> (Fe1–N2)	2.060(5)	1.896(4)	2.098(4)	2.115(3)	1.907(4)
<i>d</i> (Fe1–N3)	2.161(5)	1.963(4)	2.159(5)	2.203(3)	1.981(4)
<i>d</i> (Fe1–N4)	2.129(6)	1.960(4)	2.149(4)	2.159(3)	1.956(4)
<i>d</i> (Fe1–N5)	2.067(5)	1.901(4)	2.088(4)	2.136(3)	1.901(4)
<i>d</i> (Fe1–N6)	2.160(6)	1.977(4)	2.194(4)	2.218(3)	1.978(5)
Average	2.12	1.94	2.14	2.17	1.95

**Table 3.** N–Fe–N bond angles ( $\phi$ ) in ° for [Fe(X-pybox)<sub>2</sub>](ClO<sub>4</sub>)<sub>2</sub> (X = H, Cl, CH<sub>3</sub>O, CH<sub>3</sub>S).

X	H (400 K)	Cl (100 K)	Cl (400 K)	CH <sub>3</sub> O (100 K)	CH <sub>3</sub> S (100 K)
$\phi$ (N1–Fe1–N2)	75.2(2)	79.55(17)	74.14(16)	74.73(12)	78.90(18)
$\phi$ (N1–Fe1–N3)	150.8(2)	159.31(17)	148.07(18)	147.31(12)	158.41(18)
$\phi$ (N1–Fe1–N4)	96.0(2)	92.36(15)	92.48(15)	103.25(12)	93.7(2)
$\phi$ (N1–Fe1–N5)	105.6(2)	97.50(16)	102.35(16)	116.23(12)	104.09(18)
$\phi$ (N1–Fe1–N6)	91.5(2)	93.41(16)	95.74(16)	88.78(12)	89.80(19)
$\phi$ (N2–Fe1–N3)	75.5(2)	79.76(17)	73.93(17)	73.65(12)	79.53(18)
$\phi$ (N2–Fe1–N4)	105.9(2)	101.08(16)	105.09(15)	125.05(12)	98.96(19)
$\phi$ (N2–Fe1–N5)	177.6(2)	177.03(16)	176.50(15)	156.74(12)	176.62(19)
$\phi$ (N2–Fe1–N6)	102.8(2)	99.94(17)	105.62(16)	87.91(12)	102.61(19)
$\phi$ (N3–Fe1–N4)	91.17(19)	91.28(15)	95.20(16)	88.33(12)	89.0(2)
$\phi$ (N3–Fe1–N5)	103.7(2)	103.19(16)	109.57(18)	96.25(12)	97.45(18)
$\phi$ (N3–Fe1–N6)	95.7(2)	90.46(16)	93.30(17)	98.11(12)	95.55(19)
$\phi$ (N4–Fe1–N5)	76.4(2)	79.34(16)	74.76(15)	74.30(12)	79.4(2)
$\phi$ (N4–Fe1–N6)	158.89(18)	158.89(18)	149.28(16)	146.72(12)	158.42(18)
$\phi$ (N5–Fe1–N6)	79.78(18)	79.78(18)	74.58(15)	72.55(12)	79.10(19)

### 2.3. Magnetic Properties of Polycrystalline Specimens

The magnetic susceptibilities of polycrystalline specimens of [Fe(X-pybox)<sub>2</sub>](ClO<sub>4</sub>)<sub>2</sub> were measured on a SQUID magnetometer in a temperature range of 10–400 K. As Figure 1 shows, the high temperature limit of the  $\chi_m T$  value was 3.5–4.0 cm<sup>3</sup>·K·mol<sup>−1</sup>, being compatible with the *S* = 2 HS state of the iron(II) ion. On cooling, the  $\chi_m T$  value of [Fe(H-pybox)<sub>2</sub>](ClO<sub>4</sub>)<sub>2</sub> gradually decreased and reached practically null below 270 K. Though the  $\chi_m T$  value did not reach the high-temperature limit even at 400 K, the present SCO behavior is supposed to reproduce well the reported data (*T*<sub>1/2</sub> = 345 K [25]). Similarly, [Fe(X-pybox)<sub>2</sub>](ClO<sub>4</sub>)<sub>2</sub> (X = Cl, Ph, CH<sub>3</sub>S) showed SCO, and the transition temperatures (*T*<sub>1/2</sub>) were determined to be 310, 230, and 330 K for X = Cl, Ph, and CH<sub>3</sub>S, respectively. The CH<sub>3</sub>O derivative possessed the HS state in all the temperature range investigated here.

The CH<sub>3</sub>S derivative exhibited a  $\chi_m T$  jump at 350 K. After the jump, the  $\chi_m T$  profile never reproduced the original one because of the loss of the solvent molecules. The crystal structure analysis of the specimen after the thermal cycle was unsuccessful, and the solvent loss was confirmed by the elemental and spectroscopic analyses. We can exclude possibility that the  $\chi_m T$  increase would dominantly come from the solvent discharge “reaction”. In the present case, from a close look, the  $\chi_m T$  reached the half level before the jump, so the  $T_{1/2}$  can be correctly defined to be 330 K before the reaction. However, only the solvated form was structurally characterized and will be incorporated to the magneto-structure discussion, implying that the  $T_{1/2}$  data of [Fe(CH<sub>3</sub>S-pybox)<sub>2</sub>](ClO<sub>4</sub>)<sub>2</sub> involved the effect of the solvation.

Figure 2b depicts the plot of  $T_{1/2}$  against the Hammett substituent constant  $\sigma_p$  (−0.27, −0.01, 0, 0.00, 0.23 for the CH<sub>3</sub>O, Ph, H, CH<sub>3</sub>S, and Cl groups, respectively) [31]. No SCO appeared in the  $\chi_m T(T)$  profile of the CH<sub>3</sub>O derivative. To incorporate this result into the present discussion, it is enough to suppose that the  $G(T)$  level crossing temperature between the HS and LS states must be located much below those of the H, Cl, Ph, and CH<sub>3</sub>S derivatives (230–350 K). Therefore, we can safely conclude a positive relationship, which indicates that electron-donating groups suppress  $T_{1/2}$  while electron-withdrawing groups raise  $T_{1/2}$ . In Figure 2b, The CH<sub>3</sub>O data point has tentatively been placed at 0 K. This trend is qualitatively compatible with that of the 1-bpp series [Fe(X-1-bpp)<sub>2</sub>](BF<sub>4</sub>)<sub>2</sub> (X-1-bpp = 4-X-substituted 1-bpp) [32]. The rigid crystal lattice may play a role of a spin-transition inhibitor. The conclusion seems to have an approximate meaning, because the various space groups and molecular packing motifs were found but neglected in the above discussion.

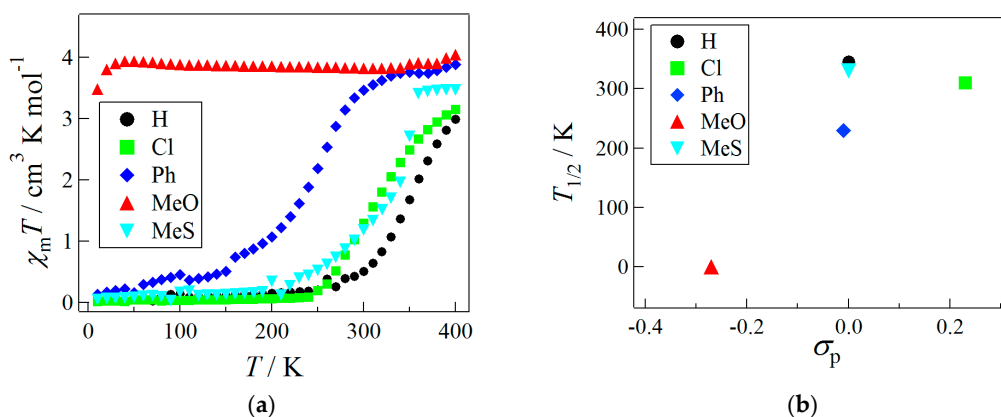


**Figure 2.** (a) Temperature dependence of  $\chi_m T$  for polycrystalline [Fe(X-pybox)<sub>2</sub>](ClO<sub>4</sub>)<sub>2</sub> measured at 5000 Oe; (b) The spin transition temperature  $T_{1/2}$  as a function of the Hammett substituent constant  $\sigma_p$ . The CH<sub>3</sub>O data point is tentatively placed at 0 K.

#### 2.4. Magnetic Properties of Solution Specimens

In solution, many of the problems from intermolecular interactions in various crystal lattices are removed, so the intrinsic intramolecular substituent effect can be extracted from variable-temperature experiments. We carried out solution susceptometry for the present complexes, inspired by the work on [Fe(X-1-bpp)<sub>2</sub>](BF<sub>4</sub>)<sub>2</sub> by Halcrow and co-workers [32]. They utilized the Evans method, but we applied the conventional SQUID apparatus. The results of the acetone-solution magnetic susceptibility measurements are summarized in Figure 3a. The data were acquired on cooling until the solution was solidified. We have found no indication of possible ligand-iron ion dissociation reaction. The  $T_{1/2}$ 's were determined as 260, 270, 240, 170, and 210 K for [Fe(X-pybox)<sub>2</sub>](ClO<sub>4</sub>)<sub>2</sub> with X = H, Cl, Ph, CH<sub>3</sub>O, and CH<sub>3</sub>S, respectively. The CH<sub>3</sub>O derivatives exhibited a remarkable difference between the solid-state and solution data; namely, the HS state at any temperature in the solid state, whereas  $T_{1/2} = 170$  K was characterized in the acetone solution. The broad transition widths observed are consistent with the complete absence of cooperativity.

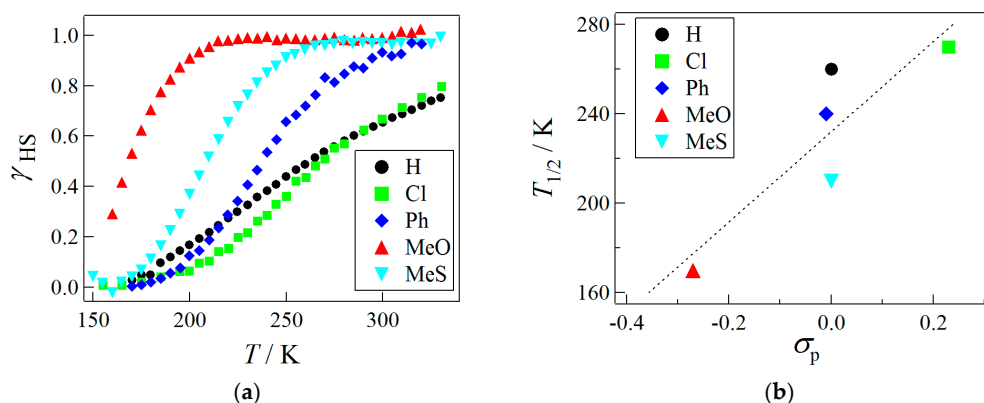


**Figure 3.** (a) Temperature dependence of the HS (high-spin) molar fraction  $\gamma_{\text{HS}}$  for acetone solutions of  $[\text{Fe}(\text{X-pybox})_2](\text{ClO}_4)_2$ , measured at 5000 Oe. (b) The spin transition temperature  $T_{1/2}$  as a function of the Hammett substituent constant  $\sigma_p$ . A dotted line represents the best linear fit.

Similarly to the solid-state experiments, we plotted the solution  $T_{1/2}$  against the Hammett substituent constant  $\sigma_p$  [31] (Figure 3b). We can easily find a positive relationship, which indicates that electron-donating groups suppress  $T_{1/2}$  while electron-withdrawing groups raise  $T_{1/2}$ . An empirical relationship equation is described with Equation (1) (a line in Figure 3b). This trend is similar to that of the 1-bpp series [32]. The solution data have the advantage of negligible intermolecular interaction. However, no structural information is afforded from the solution experiment.

$$T_{1/2} = 200(60) \text{ K} \cdot \sigma_p + 230(10) \text{ K} \quad (1)$$

### 3. Discussion

#### 3.1. Substituent Effect

In the present study, the Hammett substituent constants are available to explain the static electronic effect from substituents [33]. There are two major electronic effects from substituents: inductive effect along the  $\sigma$  electron network and mesomeric effect along the  $\pi$  electron network. The 4-position in a pyridine ring is preferable for the mesomeric effect from the pyridine nitrogen site (i.e., the 1-position). Applying the Hammett  $\sigma_p$  constant is reasonable in this system. The  $\pi$ -electron-withdrawing group stabilizes the LS state. This is because the increase of  $\pi$  electron delocalization into the ligand leads to an increase in the ligand-field splitting parameter [34,35]. In other words, the iron(II)  $t_{2g}$  orbitals are stabilized owing to the  $d\pi$ - $p\pi$  orbital interaction, and the ligand-field splitting is enhanced.

#### 3.2. Coordination Structure Effect

The HS states are known to favor distorted coordination geometry in general [34–39], which is related to long Fe–N distances and also accommodation of steric congestion during transition. From the N–Fe–N bond angles summarized in Table 3, we can calculate the  $\Sigma$  value [37] for estimation of distortion degree (Table 4), according to Equation (2). An ideal octahedron (Oh) possesses  $\Sigma = 0^\circ$ . Other popular parameters are also listed in Table 4. The  $\Theta$  value represents the deviation of the coordination geometry from an octahedron to a trigonal prism [38]. An ideal trigonal antiprism viewed from the principal axis contributes null, and an ideal Oh leads to  $\Theta = 0^\circ$ . The  $\alpha$  value is the average of the four N–Fe–N bite angles [39]. By using the SHAPE software [40], the continuous shape measures (CShM) are calculated with respect to an Oh. An ideal Oh returns null. The  $\phi$  ( $\text{N}_{\text{py}}\text{-Fe-N}_{\text{py}}$  angle) and  $\theta$  (dihedral angle between two pybox systems) values are measures of the angular Jahn–Teller distortion, as Halcrow et al. proposed to describe the criterion of SCO  $[\text{Fe}(\text{X-1-bpp})_2]^{2+}$  and related compounds [14]. Very recently, a new empirical rule has been proposed based on the interatomic N–N distance in the chelatable diimine structure [36]. Since there is no structural data of the free ligands,

the distances were calculated with the density functional theory on the b3lyp/6-311+G(2d,p) level in Gaussian 03 [41].

$$\sum = \sum_{i=1}^{12} |(\angle_{cis} N - Fe - N)_i - 90^\circ| \quad (2)$$

**Table 4.** Distortion parameters for  $[\text{Fe}(\text{X-pybox})_2](\text{ClO}_4)_2$  (X = H, Cl, CH<sub>3</sub>O, CH<sub>3</sub>S).

Parameters <sup>a</sup>	H <sup>b</sup>	Cl	CH <sub>3</sub> O	CH <sub>3</sub> S
T/K	173	400 <sup>c</sup>	100	400 <sup>c</sup>
Σ/°	90.1	130.3	90.8	142.0
Θ/°	293	417	310	455
α/°	79.7	75.5	79.6	74.4
CShM (Oh)	2.224	4.327	2.283	5.019
φ/°	179.14(11)	177.6(2)	177.03(16)	176.50(15)
θ/°	92.5	95.12(7)	91.06(4)	93.04(5)
<i>d</i> <sub>calc.</sub> (N–N)/Å <sup>d</sup>	2.855		2.854	2.854

<sup>a</sup> For the definition, see the text. <sup>b</sup> The 173 K structural data are taken from Ref. [25]. <sup>c</sup> The  $\chi_m T$  vs.  $T$  plot indicates the spin-crossover is not completed even at 400 K, so the 400 K data imply the “almost” high-spin (HS) data.

<sup>d</sup> An averaged value from two distances in a metal-free ligand. CShM: continuous shape measure; Oh: octahedron.

The geometrical parameters of the CH<sub>3</sub>O derivative could be obtained only for the HS state. Accordingly, the X = CH<sub>3</sub>O coordination structure at 100 K was compared with the X = H and Cl structures at 400 K, and the highest degree of distortion was found in the CH<sub>3</sub>O derivative, as indicated with the distortion parameters (Table 4) as well as the determined molecular structure (Figure 1c). As for the LS states, when the X = Cl and CH<sub>3</sub>S structures at 100 K were compared with the X = H structure at 173 K, their distortions were comparable to each other. These findings are confirmed by the parameters; in particular, Σ and CShM seem to be sensitive and convenient metrics. The φ and θ values of the HS  $[\text{Fe}(\text{CH}_3\text{O-pybox})_2](\text{ClO}_4)_2$  predict that this compound is not an SCO compound, and in fact it was found to be an HS compound in the whole temperature range (Figure 2a). On the other hand, the calculated N–N distance is insensitive to the substitution. As Figure 4a exemplifies, the CShM vs.  $\sigma_p$  plot has a relation with a negative slope, implying that the electron-donating group would favor a distorted structure. Such distortion would bring about preference for the HS states due to reduction of the ligand-field strength [42–45] and suppress the SCO temperature. Gao and co-workers have already reported the SCO study on a  $[\text{Fe}(\text{H-pybox})_2]^{2+}$  series with counter anion and solvent variation [25] with the substituent X fixed to H, and the magneto-structural relation was clarified to give a partially similar conclusion: highly distorted structures are favorable for the HS state and only intermediately distorted compounds show SCO.

As Figure 2 displays, although the difference of molecular packing motif is ignored, the intramolecular substituent effects seem to be dominant and approximately regulate the overall  $T_{1/2}$  trend in the solid state. As for  $[\text{Fe}(\text{CH}_3\text{O-pybox})_2](\text{ClO}_4)_2$ , the CH<sub>3</sub>O substituent brings about an excessive effect through the coordination structure distortion, as indicated by the drastic difference from the solution result. The substituents regulate both geometry and ligand-field strength. The plot of  $T_{1/2}$  for  $[\text{Fe}(\text{X-1-bpp})_2](\text{BF}_4)_2$  against  $T_{1/2}$  for  $[\text{Fe}(\text{X-pybox})_2](\text{ClO}_4)_2$  displayed a positive correlation (Figure 4b). The platforms are different, but the common substituent effect is still observable. Consequently, the SCO characteristics can be discussed in connection with the substituent effect. We have to pay attention to an indirect mechanism, where the substituent effect is operative through geometrical modification and coordination structure distortion, together with the direct mechanism from the electronic substituent effect.

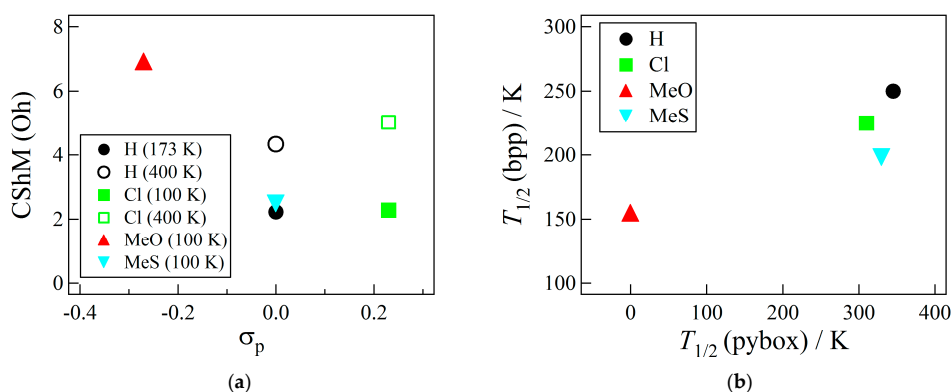


**Figure 4.** Relations between (a) the distortion parameter CShM (continuous shape measures) and Hammett substituent constant  $\sigma_p$ . (b) Plot of  $T_{1/2}$  for polycrystalline  $[\text{Fe}(\text{X}-1\text{-bpp})_2](\text{ClO}_4)_2$  vs.  $T_{1/2}$  for solution  $[\text{Fe}(\text{X}-\text{pybox})_2](\text{BF}_4)_2$ . The  $[\text{Fe}(\text{X}-1\text{-bpp})_2](\text{BF}_4)_2$  data are taken from Ref. [32].

### 3.3. Electronic Substituent Effect

The intrinsic intramolecular substituent effect can be extracted from the solution data. The results on the solution SQUID susceptometry for  $[\text{Fe}(\text{X}-\text{pybox})_2](\text{ClO}_4)_2$  ( $\text{X} = \text{H}, \text{Cl}, \text{Ph}, \text{CH}_3\text{O}, \text{CH}_3\text{S}$ ) are summarized in Figure 3a. The solution  $T_{1/2}$  vs.  $\sigma_p$  plot displays a positive relationship (Figure 3b). The solution data have no structural information, and the coordination structures might be modified by the substituent effects. However, we can assume that structural distortion would be minor from thinking of the vast conformational freedom in solution. Thus, the solution results seem to be more reliable than those of the solid-state experiments to evaluate substituent effect. The conclusion is derived here, which is basically the same as the solid-state experiments. Electron-donating groups stabilize the HS state, whereas electron-withdrawing groups stabilize the LS one.

The plot of  $T_{1/2}$  of  $[\text{Fe}(\text{X}-1\text{-bpp})_2](\text{BF}_4)_2$  in acetone solutions against the solution  $T_{1/2}$  of  $[\text{Fe}(\text{X}-\text{pybox})_2](\text{ClO}_4)_2$  displayed a positive correlation (Figure 5). This relationship is more evident than that of Figure 4b, because both were acquired in solutions. An empirical relationship is formulated as Equation (3) and superposed in Figure 5. In the doubly meridional chelated systems involving 4-X-1-dpp and 4-X-pybox, the structural distortion effects would be similar to each other. Such distortion effects are assumed to be cancelled out in the comparison analysis; the linear relationship observed here is accounted for in terms of the essential electronic substituent effect represented by the Hammett substituent constant  $\sigma_p$ .

$$T_{1/2}(\text{pybox}) = 1.10(4) \cdot T_{1/2}(\text{bpp}) \quad (3)$$

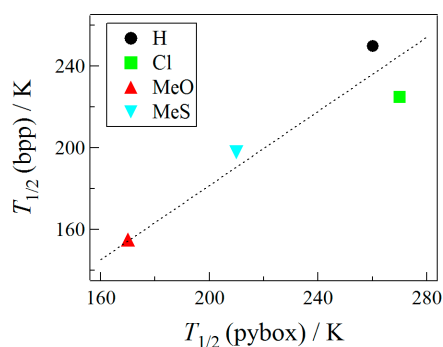


**Figure 5.** Plot of  $T_{1/2}$  for solution  $[\text{Fe}(\text{X}-1\text{-bpp})_2](\text{ClO}_4)_2$  vs.  $T_{1/2}$  for solution  $[\text{Fe}(\text{X}-\text{pybox})_2](\text{BF}_4)_2$ . The  $[\text{Fe}(\text{X}-1\text{-bpp})_2](\text{BF}_4)_2$  data are taken from Ref. [32]. A dotted line represents the best linear fit.

## 4. Experimental Section

### 4.1. Materials

Caution! We have not yet encountered any hazard, but the perchlorate salts should be handled with care.

The ligands X-pybox (X = H [23], Cl [28], Ph [29], and CH<sub>3</sub>O [30]) were prepared according to the known procedure. A new derivative CH<sub>3</sub>S-pybox was prepared according to the known procedure for the CH<sub>3</sub>O-pybox [30] with modification. A mixture of Cl-pybox (0.3707 g; 1.47 mmol) and sodium methylthiolate (0.1212 g; 1.73 mmol) in dry *N,N*-dimethylformamide was stirred at 40 °C for 12 h. After being cooled, the mixture was poured into aqueous NaHCO<sub>3</sub>, and organic substrates were extracted with ethyl acetate. The organic layer was washed with aqueous NaHCO<sub>3</sub>, dried over MgSO<sub>4</sub>, and filtered. Concentration of the filtrate gave CH<sub>3</sub>S-pybox (0.4266 g; 1.34 mmol) in 91% yield as a colorless solid. m.p. 193–195 °C. <sup>1</sup>H NMR (ECA-500, JEOL, Tokyo, Japan) (500 MHz, CDCl<sub>3</sub>) δ 7.95 (2H, s), 4.53 (4H, t, *J* = 9.6 Hz), 4.11 (4H, t, *J* = 9.6 Hz), 2.18 (3H, s). <sup>13</sup>C NMR (126 MHz, CDCl<sub>3</sub>) δ 163.53, 152.87, 146.27, 121.26, 68.47, 55.09, 13.96. MS (ESI<sup>+</sup>) (JMS-T100 AccuTOF, JEOL, Tokyo, Japan) *m/z* 286.03 (M + Na<sup>+</sup>), 264.05 (M + H<sup>+</sup>). IR (neat, attenuated total reflection (ATR)) (Nicolet 6700, Thermo Scientific, San Jose, CA, USA) 1638, 1572, 1382, 1122, 942, 868, 786, 670, 533 cm<sup>-1</sup>.

The target complexes were prepared as follows. A mixture of Cl-pybox (0.0559 g; 0.226 mmol), Fe(ClO<sub>4</sub>)<sub>2</sub>·6H<sub>2</sub>O (0.0211 g; 0.113 mmol), and L-ascorbic acid (11 mg) in methanol (18 mL) was allowed to stand in a refrigerator for 24 h. The filtration gave 0.039 g (0.052 mmol) of [Fe(Cl-pybox)<sub>2</sub>](ClO<sub>4</sub>)<sub>2</sub>. Yield 47%. m.p. 204 °C (dec.). The product was purified by recrystallization from methanol prior to the elemental and spectroscopic analyses, crystallographic analysis, and magnetic study. IR (neat, ATR) 1612, 1499, 1274, 1033, 926, 760, 651 cm<sup>-1</sup>. Anal. Calcd. for C<sub>22</sub>H<sub>20</sub>Cl<sub>4</sub>FeN<sub>6</sub>O<sub>12</sub>: C, 34.86%; H, 2.66%; N, 11.09%. Found: C, 35.02%; H, 2.55%; N, 11.37%.

Similarly, compounds [Fe(X-pybox)<sub>2</sub>](ClO<sub>4</sub>)<sub>2</sub> (X = Ph, CH<sub>3</sub>O, and CH<sub>3</sub>S) were prepared, and the yields were 44%, 26%, and 90%, respectively. [Fe(Ph-pybox)<sub>2</sub>](ClO<sub>4</sub>)<sub>2</sub>·H<sub>2</sub>O: m.p. 209 °C (dec.). IR (neat, ATR) 1584, 1374, 1269, 1068, 913, 757, 620 cm<sup>-1</sup>. Anal. Calcd. for C<sub>34</sub>H<sub>30</sub>Cl<sub>2</sub>FeN<sub>6</sub>O<sub>12</sub>·H<sub>2</sub>O: C, 47.16%; H, 4.07%; N, 9.43%. Found: C, 47.04%; H, 3.55%; N, 9.48%. [Fe(CH<sub>3</sub>O-pybox)<sub>2</sub>](ClO<sub>4</sub>)<sub>2</sub>: m.p. 289 °C (dec.). IR (neat, ATR) 1587, 1372, 1239, 1072, 916, 859, 620, 578 cm<sup>-1</sup>. Anal. Calcd. for C<sub>24</sub>H<sub>26</sub>Cl<sub>2</sub>FeN<sub>6</sub>O<sub>14</sub>: C, 38.47%; H, 3.50%; N, 11.22%. Found: C, 38.53%; H, 3.29%; N, 11.16%. [Fe(CH<sub>3</sub>S-pybox)<sub>2</sub>](ClO<sub>4</sub>)<sub>2</sub>·2CH<sub>3</sub>OH: m.p. 208 °C (dec.). IR (neat, ATR) 1574, 1485, 1372, 1270, 1069, 915, 796, 619 cm<sup>-1</sup>. Anal. Calcd. for C<sub>24</sub>H<sub>26</sub>Cl<sub>2</sub>FeN<sub>6</sub>O<sub>12</sub>S<sub>2</sub>·CH<sub>4</sub>O·H<sub>2</sub>O: C, 36.11%; H, 3.88%; N, 10.11%; S, 7.71%. Found: C, 36.14%; H, 3.58%; N, 10.08%; S, 7.70%. After thermal treatment at 400 K in a SQUID magnetometer. Anal. Calcd. for C<sub>24</sub>H<sub>26</sub>Cl<sub>2</sub>FeN<sub>6</sub>O<sub>12</sub>S<sub>2</sub>: C, 36.89%; H, 3.35%; N, 10.76%; S, 8.21%. Found: C, 36.56%; H, 3.18%; N, 10.60%; S, 8.19%.

### 4.2. Crystallographic Analysis

X-Ray diffraction data of [Fe(X-pybox)<sub>2</sub>](ClO<sub>4</sub>)<sub>2</sub> (X = H, Cl, CH<sub>3</sub>O, CH<sub>3</sub>S) were collected on a Saturn70 CCD diffractometer (Rigaku, Tokyo, Japan) with graphite monochromated Mo K $\alpha$  radiation ( $\lambda$  = 0.71073 Å). The structures were directly solved by a heavy-atom method and expanded using Fourier techniques in the CRYSTALSTRUCTURE [46]. Numerical absorption correction was used. Hydrogen atoms were located at calculated positions, and their parameters were refined as a riding model. The thermal displacement parameters of non-hydrogen atoms were refined anisotropically. Selected crystallographic data are given in Table 1, and selected bond distances and angles are listed in Tables 2 and 3, respectively. CCDC numbers 1559025, 1559026, 1559027, 1559028, and 1559029 for [Fe(X-pybox)<sub>2</sub>](ClO<sub>4</sub>)<sub>2</sub> (X = H, Cl (100 K), Cl (400 K), CH<sub>3</sub>O, CH<sub>3</sub>S, respectively) include the experimental details and full geometrical parameter tables. These data can be obtained free of charge via <http://www.ccdc.cam.ac.uk/conts/retrieving.html>.

### 4.3. Magnetic Study

Magnetic susceptibilities of  $[\text{Fe}(\text{X-pybox})_2](\text{ClO}_4)_2$  ( $\text{X} = \text{H}, \text{Cl}, \text{Ph}, \text{CH}_3\text{O}, \text{CH}_3\text{S}$ ) were measured on a Quantum Design MPMS-XL7 SQUID magnetometer (San Diego, CA, USA) with a static field of 0.5 T. The magnetic responses were corrected with diamagnetic blank data of the sample holder measured separately. The diamagnetic contribution of the sample itself was estimated from Pascal's constants. The solution magnetic susceptibilities were measured in the same SQUID apparatus. The specimen was dissolved in acetone, and the resultant clear solution was transferred into a 5 mm- $\phi$  NMR sample tube. After the solution was degassed with argon gas bubbling, the sample tube was sealed and mounted in a SQUID probe. The susceptibility data were acquired on cooling until the acetone solution was solidified (typically around 160 K). In the analysis, the diamagnetic contribution was numerically estimated as a temperature-independent susceptibility term, so that the  $\chi_m T$  values of the LS and/or HS regions should be almost constant. Owing to the ambiguity of the sample amount, the S-shaped profile was drawn on the molar fraction basis,  $\gamma_{\text{HS}} = x(\text{HS})/(x(\text{HS}) + x(\text{LS}))$  against temperature.

### 4.4. DFT Calculation Study

Density-functional-theory (DFT) calculation was performed by using the Gaussian 03 package [41]. The geometry was optimized after the b3lyp Hamiltonian and the 6-311+G(2d,p) basis set were chosen. The convergence criterion was below  $10^{-8}$  a.u. in the self-consistent field energy.

## 5. Conclusions

We synthesized four new iron(II) complexes (Cl, Ph,  $\text{CH}_3\text{O}$ , and  $\text{CH}_3\text{S}$ ). The SCO transition temperature  $T_{1/2}$  can be changed by introducing a substituent at the 4-position of the pyridine ring. The  $T_{1/2}$  around or slightly above room temperature may be very attractive for future application of the SCO materials. In the solid-state study, there seems to be a correlation between  $\sigma_p$  and  $\Sigma$  or  $\sigma_p$  and CShM, and furthermore between  $\sigma_p$  and  $T_{1/2}$ . The coordination structure distortion depends on the substituents, and the distortion also indirectly regulates  $T_{1/2}$ . Distorted structures stabilize the HS state. In the solution study, the substituent dependence on  $T_{1/2}$  became very obvious, and electron-donating groups stabilize the HS state. The SCO temperature is regulated by the substituents, being similar to the known parallel work on  $[\text{Fe}(\text{X-1-bpp})_2](\text{BF}_4)_2$ . The platforms are different, but the SCO characteristics can be discussed in connection with the substituent effect in a generalized manner.

**Acknowledgments:** This work was financially supported from KAKENHI (JSPS/15H03793).

**Author Contributions:** Akifumi Kimura participated in the preparation, X-ray structural analysis, and magnetic study. Takayuki Ishida designed the study and wrote the manuscript.

**Conflicts of Interest:** The authors declare no conflict of interest.

## References

1. Gütlich, P.; Goodwin, H.A. (Eds.) *Spin Crossover in Transition Metal Compounds I, II, and III*; Springer: Berlin, Germany, 2004.
2. Gütlich, P.; Gaspar, A.B.; Garcia, Y. Spin state switching in iron coordination compounds. *Beilstein J. Org. Chem.* **2013**, *9*, 342–391. [[CrossRef](#)] [[PubMed](#)]
3. Halcrow, M.A. *Spin-Crossover Materials: Properties and Applications*; John Wiley & Sons, Ltd.: Oxford, UK, 2013.
4. Halcrow, M.A. Spin-Crossover compounds with wide thermal hysteresis. *Chem. Lett.* **2014**, *43*, 1178–1188. [[CrossRef](#)]
5. Kahn, O. Chapter 4. In *Molecular Magnetism*; VCH: Weinheim, Germany, 1993.
6. Harding, D.J.; Harding, P.; Phonsri, W. Spin crossover in iron(III) complexes. *Coord. Chem. Rev.* **2016**, *313*, 38–61. [[CrossRef](#)]
7. Letard, J.-F.; Guionneau, P.; Nguyen, O.; Costa, J.S.; Marcen, S.; Chastanet, G.; Marchivie, M.; Goux-Capes, L. A guideline to the design of molecular-based materials with long-lived photomagnetic lifetimes. *Chem. Eur. J.* **2005**, *11*, 4582–4589. [[CrossRef](#)] [[PubMed](#)]

8. Letard, J.-F.; Guionneau, P.; Godjovi, E.; Lavastre, O.; Bravic, G.; Chasseau, D.; Kahn, O. Wide Thermal Hysteresis for the Mononuclear Spin-Crossover Compound *cis*-Bis(thiocyanato)bis[*N*-(2'-pyridylmethylene)-4-(phenylethynyl)anilino]iron(II). *J. Am. Chem. Soc.* **1997**, *119*, 10861–10862. [[CrossRef](#)]
9. Yamada, M.; Hagiwara, H.; Torigoe, H.; Matsumoto, N.; Kojima, M.; Dahan, F.; Tuchagues, J.P.; Re, N.; Iijima, S. A variety of spin-crossover behaviors depending on the counter anion: Two-dimensional complexes constructed by NH $\cdots$ Cl $^-$  hydrogen bonds, [(Fe $^{II}$ H $_3$ LMe)]Cl $\cdot$ X (X = PF $_6^-$ , AsF $_6^-$ , SbF $_6^-$ , CF $_3$ SO $_3^-$ ; H $_3$ LMe = tris[2-[(2-methylimidazol-4-yl)methylidene]amino]ethyl]amine). *Chem. Eur. J.* **2006**, *12*, 4536–4549. [[PubMed](#)]
10. Takahashi, K.; Kawakami, T.; Gu, Z.; Einaga, Y.; Fujishima, A.; Sato, O. An abrupt spin transition based on short S...S contacts in a novel Fe(II) complex whose ligand contains a 1,3-dithiole ring. *Chem. Commun.* **2003**, 2374–2375. [[CrossRef](#)]
11. Mochida, N.; Kimura, A.; Ishida, T. Spin-Crossover Hysteresis of [Fe $^{II}$ (L $_H^{iPr}$ ) $_2$ (NCS) $_2$ ] (L $_H^{iPr}$  = *N*-2-Pyridylmethylene-4-isopropylaniline Accompanied by Isopropyl Conformation Isomerism. *Magnetochemistry* **2015**, *1*, 17–27. [[CrossRef](#)]
12. Oso, Y.; Ishida, T. Spin-crossover transition in a mesophase iron(II) thiocyanate complex chelated with 4-hexadecyl-*N*-(2-pyridylmethylene)aniline. *Chem. Lett.* **2009**, *38*, 604–605. [[CrossRef](#)]
13. Oso, Y.; Kanatsuki, D.; Saito, S.; Nogami, T.; Ishida, T. Spin-crossover transition coupled with another solid-solid phase transition for iron(II) thiocyanate complexes chelated with alkylated *N*-(di-2-pyridylmethylene)anilines. *Chem. Lett.* **2008**, *37*, 760–761. [[CrossRef](#)]
14. Halcrow, M.A. Iron(II) complexes of 2,6-di(pyrazol-1-yl)pyridines—A versatile system for spin-crossover research. *Coord. Chem. Rev.* **2009**, *253*, 2493–2514. [[CrossRef](#)]
15. Craig, G.A.; Roubeau, O.; Aromi, G. Spin state switching in 2,6-bis(pyrazol-3-yl)pyridine (3-bpp) based Fe(II) complexes. *Coord. Chem. Rev.* **2014**, *269*, 13–31. [[CrossRef](#)]
16. Krober, J.; Codjovi, E.; Kahn, O.; Groliere, F.; Jay, C. A Spin Transition System with a Thermal Hysteresis at Room Temperature. *J. Am. Chem. Soc.* **1993**, *115*, 9810–9811. [[CrossRef](#)]
17. Hirose, N.; Oso, Y.; Ishida, T. Spin-crossover and light-induced excited spin-state trapping observed for an iron(II) complex chelated with tripodal tetrakis(2-pyridyl)methane. *Chem. Lett.* **2012**, *41*, 716–718. [[CrossRef](#)]
18. Yamasaki, M.; Ishida, T. Heating-rate dependence of spin-crossover hysteresis observed in an iron(II) complex having tris(2-pyridyl)methanol. *J. Mater. Chem. C* **2015**, *3*, 7784–7787. [[CrossRef](#)]
19. Yamasaki, M.; Ishida, T. Spin-crossover thermal hysteresis and light-induced effect on iron(II) complexes with tripodal tris(2-pyridyl)methanol. *Polyhedron* **2015**, *85*, 795–799. [[CrossRef](#)]
20. Johnson, J.S.; Evans, D.A. Chiral Bis(oxazoline) Copper(II) Complexes: Versatile Catalysts for Enantioselective Cycloaddition, Aldol, Michael, and Carbonyl Ene Reactions. *Acc. Chem. Res.* **2000**, *33*, 325–335. [[CrossRef](#)] [[PubMed](#)]
21. Desimoni, G.; Faita, G.; Quadrelli, P. Pyridine-2,6-bis(oxazolines), Helpful Ligands for Asymmetric Catalysts. *Chem. Rev.* **2003**, *103*, 3119–3154. [[CrossRef](#)] [[PubMed](#)]
22. Yuasa, J.; Ohno, T.; Miyata, K.; Tsumatori, H.; Hasegawa, Y.; Kawai, T. Noncovalent Ligand-to-Ligand Interactions Alter Sense of Optical Chirality in Luminescent Tris( $\beta$ -diketonate) Lanthanide(III) Complexes Containing a Chiral Bis(oxazolonyl) Pyridine Ligand. *J. Am. Chem. Soc.* **2011**, *133*, 9892–9902. [[CrossRef](#)] [[PubMed](#)]
23. De Bettencourt-Dias, A.; Barber, P.S.; Viswanathan, S.; de Lill, D.T.; Rollett, A.; Ling, G.; Altun, S. Para-Derivatized Pybox Ligands As Sensitizers in Highly Luminescent Ln(III) Complexes. *Inorg. Chem.* **2010**, *49*, 8848–8861. [[CrossRef](#)] [[PubMed](#)]
24. De Bettencourt-Dias, A.; Barber, P.S.; Bauer, S. A Water-Soluble Pybox Derivatives and Its Highly Luminescent Lanthanide Ion Complexes. *J. Am. Chem. Soc.* **2012**, *134*, 6987–6994. [[CrossRef](#)] [[PubMed](#)]
25. Zhu, Y.-Y.; Li, H.-Q.; Ding, Z.-Y.; Lu, X.-J.; Zhao, L.; Meng, Y.-S.; Liu, T.; Gao, S. Spin transition in a series of [Fe(pybox) $_2$ ] $^{2+}$  complexes modulated by ligand structures, counter anions, and solvents. *Inorg. Chem. Front.* **2016**, *3*, 1624–1636. [[CrossRef](#)]
26. Zhu, Y.-Y.; Liu, C.-W.; Yin, J.; Meng, Z.-S.; Yang, Q.; Wang, J.; Liu, T.; Gao, S. Structural phase transition in a multi-induced mononuclear Fe $^{II}$  spin-crossover complex. *Dalton Trans.* **2015**, *44*, 20906–20912. [[CrossRef](#)] [[PubMed](#)]

27. Burrows, K.E.; McGrath, S.E.; Kulmaczewski, R.; Cespedes, O.; Barrett, S.A.; Halcrow, M.A. Spin State of Homochiral and Heterochiral Isomers of  $[\text{Fe}(\text{PyBox})_2]^{2+}$  Derivatives. *Chem. Eur. J.* **2017**, *23*, 9067–9075. [[CrossRef](#)] [[PubMed](#)]
28. De Bettencourt-Dias, A.; Rossini, J.S.K. Ligand Design for Luminescent Lanthanide-Containing Metallopolymers. *Inorg. Chem.* **2016**, *55*, 9954–9963. [[CrossRef](#)] [[PubMed](#)]
29. Yu, X.; Yang, T.; Wang, S.; Xu, H.; Gong, H. Nickel-Catalyzed Reductive Cross-Coupling of Unactivated Alkyl Halides. *Org. Lett.* **2011**, *13*, 2138–2141. [[CrossRef](#)] [[PubMed](#)]
30. Vermonden, T.; Branowska, D.; Marcelis, A.T.M.; Sudholter, E.J.R. Synthesis of 4-functionalized terdentate pyridine-based ligands. *Tetrahedron* **2003**, *59*, 5039–5045. [[CrossRef](#)]
31. Hansch, C.; Leo, A.; Taft, R.W. A survey of Hammett substituent constants and resonance and field parameters. *Chem. Rev.* **1991**, *91*, 165–195. [[CrossRef](#)]
32. Cook, L.J.K.; Rafal, K.; Mohammed, R.; Dudley, S.; Barrett, S.A.; Little, M.A.; Deeth, R.J.; Halcrow, M.A. A Unified Treatment of the Relationship Between Ligand Substituents and Spin State in a Family of Iron(II) Complexes. *Angew. Chem. Int. Ed.* **2016**, *55*, 4327–4331. [[CrossRef](#)] [[PubMed](#)]
33. Isaccs, N.S. Chapter 4. In *Physical Organic Chemistry*; Wiley: New York, NY, USA, 1987.
34. Tweedle, M.F.; Wilson, L.J. Variable Spin Iron(III) Chelates with Hexadentate Ligands Derived from Triethylenetetramine and Various Salicylaldehydes. Synthesis, Characterization, and Solution State Studies of a New  $^2T \leftrightarrow ^6A$  Spin Equilibrium System. *J. Am. Chem. Soc.* **1976**, *98*, 4824–4834. [[CrossRef](#)]
35. Takahashi, K.; Hasegawa, Y.; Sakamoto, R.; Nishikawa, M.; Kume, S.; Nishibori, E.; Nishihara, H. Solid-State Ligand-Driven Light-Induced Spin Change at Ambient Temperatures in Bis(dipyrazolylstyrylpyridine)iron(II) Complexes. *Inorg. Chem.* **2012**, *51*, 5188–5198. [[CrossRef](#)] [[PubMed](#)]
36. Phan, H.; Hrudka, J.J.; Igimbayeva, D.; Daku, L.M.L.; Shatruck, M. A Simple Approach for Predicting the Spin State of Homoleptic Fe(II) Tris-diimine Complexes. *J. Am. Chem. Soc.* **2017**, *139*, 6437–6447. [[CrossRef](#)] [[PubMed](#)]
37. Guionneau, P.; Marchivie, M.; Bravic, G.; Létard, J.-F.; Chasseau, D. Structural Aspects of Spin Crossover. Example of the  $[\text{Fe}^{\text{II}}\text{L}_n(\text{NCS})_2]$  Complexes. *Top. Curr. Chem.* **2004**, *234*, 97–128.
38. Marchivie, M.; Guionneau, P.; Létard, J.F. Photo-induced spin-transition: the role of the iron(II) environment distortion. *Acta Crystallogr. Sect. B Struct. Sci.* **1991**, *15*, 181–190. [[CrossRef](#)] [[PubMed](#)]
39. Halcrow, M.A. Structure: function relationships in molecular spin-crossover complexes. *Chem. Soc. Rev.* **2011**, *40*, 4119–4142. [[CrossRef](#)] [[PubMed](#)]
40. Llunell, M.; Casanova, D.; Circra, J.; Bofill, J.M.; Alcmay, P.; Alvarez, S.; Pinsky, M.; Avnir, D. *SHAPE*; v2.1; University of Barcelona and The Hebrew University of Jerusalem: Barcelona, Spain, 2005.
41. *Gaussian 03*; revision C.02; Gaussian Inc.: Wallingford, CT, USA, 2004.
42. Kroll, N.; Theilacker, K.; Schoknecht, M.; Baabe, D.; Wiedemann, D.; Kaupp, M.; Grohmann, A.; Hörner, G. Controlled ligand distortion and its consequences for structure, symmetry, conformation and spin-state preferences of iron(II) complexes. *Dalton Trans.* **2015**, *44*, 19232–19247. [[CrossRef](#)] [[PubMed](#)]
43. Matouzenko, G.S.; Jeanneau, E.; Verat, A.Y.; de Gaetano, Y. The Nature of Spin Crossover and Coordination Core Distortion in a Family of Binuclear Iron(II) Complexes with Bipyridyl-Like Bridging Ligands. *Eur. J. Inorg. Chem.* **2012**, 969–977. [[CrossRef](#)]
44. Cook, L.J.K.; Thorp-Greenwood, F.L.; Comyn, T.P.; Cespedes, O.; Chastanet, G.; Halcrow, M.A. Unexpected Spin-Crossover and a Low-Pressure Phase Change in an Iron(II) Dipyrazolylpyridine Complex Exhibiting a High-Spin Jahn–Teller Distortion. *Inorg. Chem.* **2015**, *54*, 6319–6330. [[CrossRef](#)] [[PubMed](#)]
45. Yang, Q.; Cheng, X.; Gao, C.; Wang, B.; Wang, Z.; Gao, S. Structural Distortion Controlled Spin-Crossover Behavior. *Cryst. Growth Des.* **2015**, *15*, 2565–2567. [[CrossRef](#)]
46. *CRYSTALSTRUCTURE*, version 4.2.1; Rigaku/MS: The Woodlands, TX, USA, 2015.

